Low-lying states of ^{92,93}Nb excited in the reactions induced by the weakly-bound nucleus ^{6}Li near the Coulomb barrier*

Yi-Feng Lv(吕翌丰)[1] Jing-Bin Lu(陆景彬)[1;1)] Gao-Long Zhang(张高龙)[2,3;2)] Yi-Heng Wu(吴义恒)[4]
Cen-Xi Yuan(袁岑溪)[5] Guan-Jian Fu(傅冠健)[6] Guang-Xin Zhang(张广鑫)[2] Zhen Huang(黄珍)[2]
Ming-Li Wang(王明李)[2] Shi-Peng Hu(胡世鹏)[7] Hui-Bin Sun(孙慧斌)[7] Huan-Qiao Zhang(张焕乔)[8]
Cheng-Qian Li(李成乾)[1] Ke-Yan Ma(马克岩)[1] Ying-Jun Ma(马英君)[1] Yun-Zuo Liu(刘运祚)[1]
D. Testov[9] P. R. John[9] J. J. Valiente-Dobon[10] A. Goasduff[9] M. Siciliano[10,11]
F. Galtarossa[10] F. Recchia[9] D. Mengoni[9] D. Bazzacco[9]

[1]College of physics, Jilin University, ChangChun 130012, China
[2]School of Physics and Nuclear Energy Engineering, Beihang University, Beijing 100191, China
[3]Beijing Advanced Innovation Center for Big Data-Based Precision Medicine, Beihang University, Beijing 100083, China
[4]School of Physics and Electronic Engineering, An Qing Normal University, An qing, 246133, China
[5]Sino-French Institute of Nuclear Engineering and Technology, Sun Yat-Sen University, Zhuhai 519082, China
[6]School of Physics Science and Engineering, Tongji University, Shanghai 200092, China
[7]College of Physics and Optoelectronic Engineering, Shenzhen University, Shenzhen 518060, China
[8]China Institute of Atomic Energy, Beijing 102413, China
[9]Dipartimento di Fisica and INFN, Sezione di Padova, Padova, Italy
[10]INFN, Laboratori Nazionali di Legnaro, Legnaro (Padova), Italy
[11]Irfu/CEA, Universite de Paris-Saclay, Gif-sur-Yvette, France

Abstract: Excited states of odd-odd nucleus ^{92}Nb and odd-A nucleus ^{93}Nb were populated in the ^{6}Li+ ^{89}Y reaction with an incident energy of 34 MeV. The processes that produce ^{92,93}Nb and can be measured by a combination of light charged particle and gamma ray measurements are discussed. Twenty new transitions are observed and eight new levels are constructed in ^{92}Nb, and in addition two new transitions are added to the level scheme of ^{93}Nb. Using shell model calculations, the low-lying structure of ^{92}Nb is investigated and compared with the experimental results.

Keywords: weakly-bound projectile, coincidence measurement, level structure, odd-odd nucleus ^{92}Nb, odd-*A* nucleus ^{93}Nb.

PACS: 27.60.+j, 23.20.Lv, 25.70.Mn **DOI:** 10.1088/1674-1137/43/10/104102

1 Introduction

Over the past few years, much effort in both theory and experiment has been directed to the study of reactions induced by weakly-bound nuclei, especially the elastic scattering, breakup and fusion [1-5]. The occurrence of breakup of weakly-bound nuclei may lead to further reactions, which makes the whole reaction process more complicated [4]. ^{92,93}Nb are the residues of the ^{6}Li+^{89}Y experiment performed at LNL-INFN in Italy, with the goal of studying the reaction mechanisms of a weakly-bound nuclear system [6, 7]. In the following, the processes that produce ^{92,93}Nb nuclei and that involve fusion-evaporation and can be identified with γ-particle coincidence measurements are discussed. Since gamma-gamma coincidence measurements were performed in the present experiment, it was an opportunity to further explore the level schemes of ^{92,93}Nb.

It is well known that the level structure of nuclei N=50,51 is dominated by single-particle excitations, even for states with high spin. On the other hand, nuclei with $N \geqslant 55$ exhibit collective behavior [8, 9].

As it si a nearly spherical nucleus with N=51 in the A~90 mass region, the studies of the excited states of ^{92}Nb are of importance for establishing and testing the re-

Received 26 May 2019, Published online 3 September 2019
* Supported by National Natural Science Foundation of China (U1867210, 11775098, 11475013, U1832130 and 11775316)
1) E-mail: ljb@jlu.edu.cn
2) E-mail: zgl@buaa.edu.cn

sidual interactions in shell model calculations. Previously, the level structure of ^{92}Nb was mainly investigated by proton and ^{3}He induced reactions [10-13], and the energies of excited states were extended up to 3797 keV by the ^{88}Sr (^{7}Li, $3n$)^{92}Nb experiment [14]. Recently, high-spin states of ^{92}Nb were studied in the heavy ion fusion-evaporation reaction ^{82}Se (^{14}N,$4n$)^{92}Nb [15]. For the middle-low excited states of ^{92}Nb, the information is relatively scarce, and thus it is important to further explore this nucleus experimentally. From the theoretical point of view, ^{92}Nb was studied within the framework of the shell model, and its low-lying levels below $E_{\rm level}$=2287 keV [12] were described by taking the even-even nucleus ^{88}Sr as the inert core, while the valance nucleons occupy the $\pi p_{1/2}$, $g_{9/2}$ and $\nu d_{5/2}$ orbitals. Nevertheless, from the theoretical point of view, further study of ^{92}Nb is still necessary.

As a "transitional" nucleus with N=52, the excitation of ^{93}Nb is relative intricate [8]. In an earlier work, ^{93}Nb was studied in the (n, $n\gamma$) and (p,$2n\gamma$) reactions [16]. The I^{π}=3/2^{-} at 1840 keV and I^{π}=5/2^{-} at 2013 keV were identified as mixed-symmetry states, which can be viewed as low-energy collective modes where protons and neutrons move uncoupled. High-spin states were studied in the ^{82}Se(^{16}O, $p4n$)^{93}Nb reaction, with the level schemes up to excitation energy of 11 MeV [17]. An M1 rotational band was reported and showed the characteristics of oblate collective rotational band. The investigation of the level structure of ^{93}Nb can provide additional information for a systematic study of nuclei with N=52.

In this work, the low-lying structure of ^{92}Nb was further studied, and its proposed level scheme was calculated using the shell model code NushellX with SNE valence space, and compared with the experimental results. In addition, two new transitions were observed in ^{93}Nb, as discussed in the following section.

2 Experiment and production of ^{92,93}Nb

The study of the ^{6}Li+^{89}Y reaction was performed at LNL-INFN in Italy. A 550 μg/cm^2 ^{89}Y target, which was supported by a 340 μg/cm^2 ^{12}C foil, was bombarded by the $E_{\rm lab}$=34 MeV ^{6}Li^{3+} beam with an average intensity of 1.0 enA, provided by the Tandem-XTU accelerator. The γ-rays were detected by the GALILEO array, which is composed of 25 Compton-suppressed high-purity germanium (BGO-HPGe) detectors arranged in 4 rings: 10 at 90° and 15 at 119°, 129°, 152° with respect to the beam direction [18]. The EUCLIDES 4π Si-telescope array, which consists of 5 segmented and 35 single plates of ΔE/E Si telescopes (the thicknesses of the ΔE and E detectors are 130 μm and 1000 μm, respectively) was used to collect the emitted light charged particles [19]. The distance between the center of the Si telescopes and the center of the target was around 6.2 cm. An Al cylinder was inserted inside EUCLIDES, so that backward angles larger than 150° were unshielded. The thickness of the Al cylinder was 200 μm, so as to stop the intense scattered beam particles from destroying the Si detectors. The energy and efficiency calibrations of each Ge detector in the real geometrical conditions were performed with the following standard sources: ^{60}Co, ^{241}Am, ^{133}Ba, ^{152}Eu, ^{88}Y, covering the energy region from 39.522 keV (^{152}Eu) to 2734 keV (^{88}Y). After further delicate energy calibrations and gain matching with characteristic γ-rays of the residual nuclei, the recorded γ-γ coincidence events were sorted into a two-dimensional E_γ-E_γ symmetric matrix, and two asymmetric ADO matrices. In this experiment, about 14×10^6 γ-γ coincidence events (without any particle selection) were collected.

The fusion reaction induced by a weakly-bound projectile at near-barrier energies is complicated due to low breakup threshold [6, 20]. When the projectile completely fuses with the target nucleus without breakup (BU), the process is a direct complete fusion (DCF). When the projectiles breakup, then: 1) if all the fragments fuse with the target nucleus, the process is a sequential complete fusion (SCF); or 2) if only part of the fragments fuse with the target nucleus, the process is an incomplete fusion (ICF) [6]. In addition, when a medium-mass target nucleus is involved, the fusion process can evaporate not only neutrons but also light charged particles including protons and alpha particles. In the present experiment, ^{92}Nb can be produced in a complete fusion of ^{6}Li with the ^{89}Y target nuclei, followed by the $1p2n$ evaporation channel. As a result, the characteristic γ-rays from ^{92}Nb are in coincidence with protons emitted from the compound nucleus, as shown in Fig. 1(a). In addition, the ^{92}Mo residue from the reaction can only be produced by the CF process. The yield ratio of ^{92}Nb to ^{92}Mo (^{92}Nb/^{92}Mo) in the present experiment is around 0.38, which is larger than given by the statistical evaporation model (around 0.26). Such an increment of the ^{92}Nb/^{92}Mo ratio indicates that the ICF process may contribute to the production of ^{92}Nb. Fig. 1(b) shows the γ-ray spectrum measured in coincidence with deuterons, in which the characteristic gamma rays of ^{92}Nb are clearly visible. It is concluded that ^{92}Nb can also be populated in the ICF process of ^{6}Li, where alpha particles from the breakup of ^{6}Li fuse with the ^{89}Y target nucleus, and simultaneously, the other fragment (deuteron) escapes and is detected. In summary, the ^{92}Nb residue observed in this experiment was populated in the ^{89}Y(^{6}Li, $p2n$)^{92}Nb and ^{89}Y(α,n)^{92}Nb reactions.

The ^{93}Nb residue in the present experiment can be

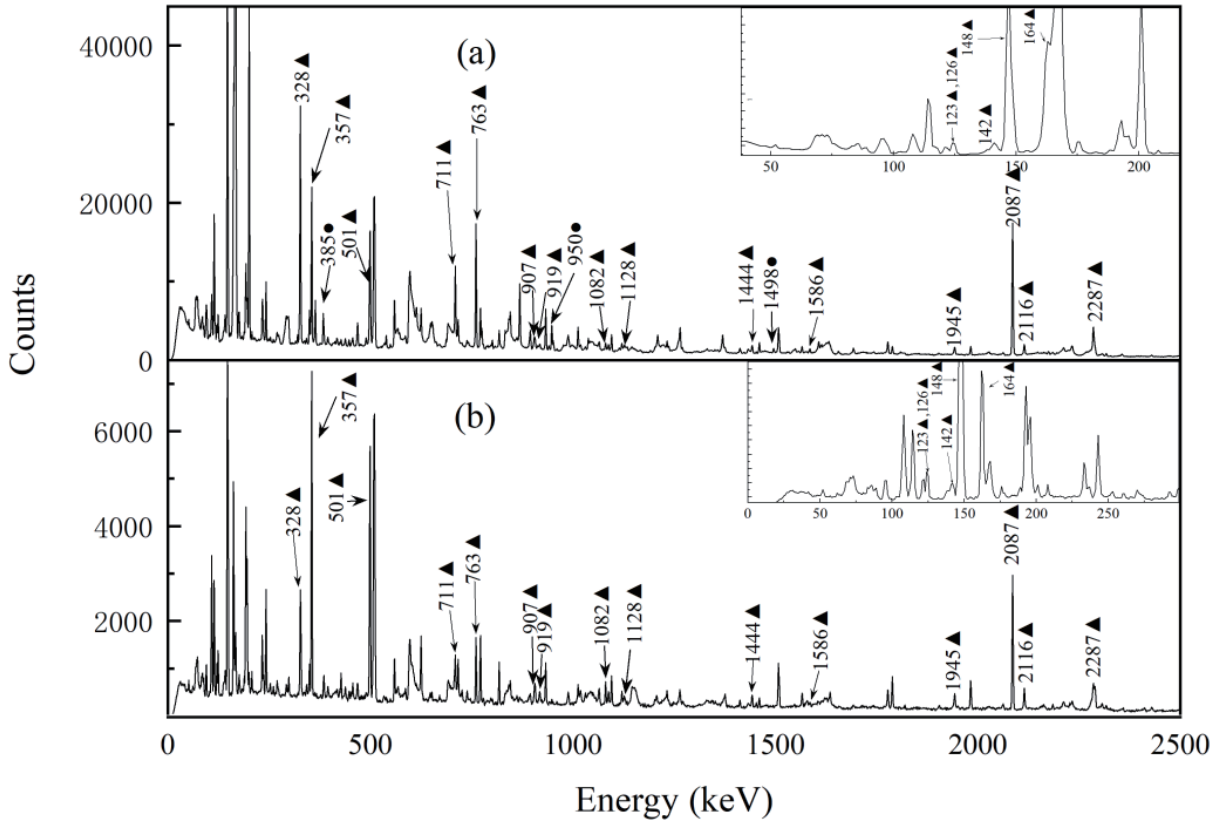

Fig. 1. γ-energy spectra in coincidence with protons (a) and deuterons (b). Representative γ-rays from ^{92}Nb and ^{93}Nb are marked with black triangles and black circles, respectively.

produced by the complete fusion of ^{6}Li with ^{89}Y, followed by the 1p1n evaporation channel, as can be seen in the proton gated spectrum shown in Fig. 1(a). The cross-section for alpha particle stripping from ^{6}Li on a ^{89}Y target producing ^{93}Nb is small, and this process can be neglected.

3 Construction of level schemes of ^{92,93}Nb

The level structure of ^{92}Nb was studied by several researchers [10-14]. The high-spin states of ^{92}Nb were recently studied in the ^{82}Se(^{14}N,4n)^{92}Nb reaction by Wu et al [15]. The projectile used in the present experiment brings lower excitation energy to the compound nucleus, so that the relatively lower excited states of ^{92}Nb can be populated and the middle-low level structure of ^{92}Nb studied. The proposed level scheme of ^{92}Nb is shown in Fig. 2, which is extended up to ~5.4 MeV excitation energy, and 20 new transitions and 8 new levels are added to ^{92}Nb. Sample coincidence spectra, gated on 2287, 387, 328 and 115 keV, are shown in Fig. 3(a)-(d). The relative intensities (I_γ) and the initial and final states (E_i^π and E_f^π) of the observed transitions in ^{92}Nb are summarized in Table 1.

In order to obtain the multipolarity of the newly observed γ-rays, the angular distributions of each γ-ray from the oriented residues (ADO) were analyzed. Assuming that γ_1 and γ_2 are the cascading transitions in the same nucleus, the ADO ratio of γ_1 is deduced by $I_{\gamma1}(152°)/I_{\gamma1}(90°)$, where $I_{\gamma1}(152°$ or $90°)$ represents the intensity of γ_1-rays collected by the detectors at 152° or 90° , and in coincidence with γ_2-rays measured by all detectors. By calculating the ADO ratio of γ-rays with known multipolarity in ^{92}Mo, ^{91}Mo, ^{92}Nb, ^{93}Nb, ^{90}Zr, ^{89}Zr produced in the present experiment, typical ADO ratios $I_\gamma(152°)/I_\gamma(90°)$ for quadrupole and dipole transitions are around 1.6 and 0.8, respectively, as shown in Fig. 4(a). The spins of the states of ^{92}Nb are assigned tentatively. For the two lower transitions, 97 and 126 keV, the intensity balance rule is used, which supports to some extent the spin assignment of the levels .

Two new transitions, 504 and 572 keV, are added to the level scheme of ^{93}Nb feeding into the 2180 keV state, as shown in Fig. 5. From the summed spectrum of 689 and 541 keV, shown in Fig. 6, the peaks of the new transitions 504 and 572 keV can be clearly seen. The ADO ratios for the two transitions are 1.45 and 0.94, indicating quadrupole and dipole properties, respectively. Therefore, the spins of the 2752 keV and 2684 keV states are assigned as 21/2, and 19/2, respectively. The relative in-

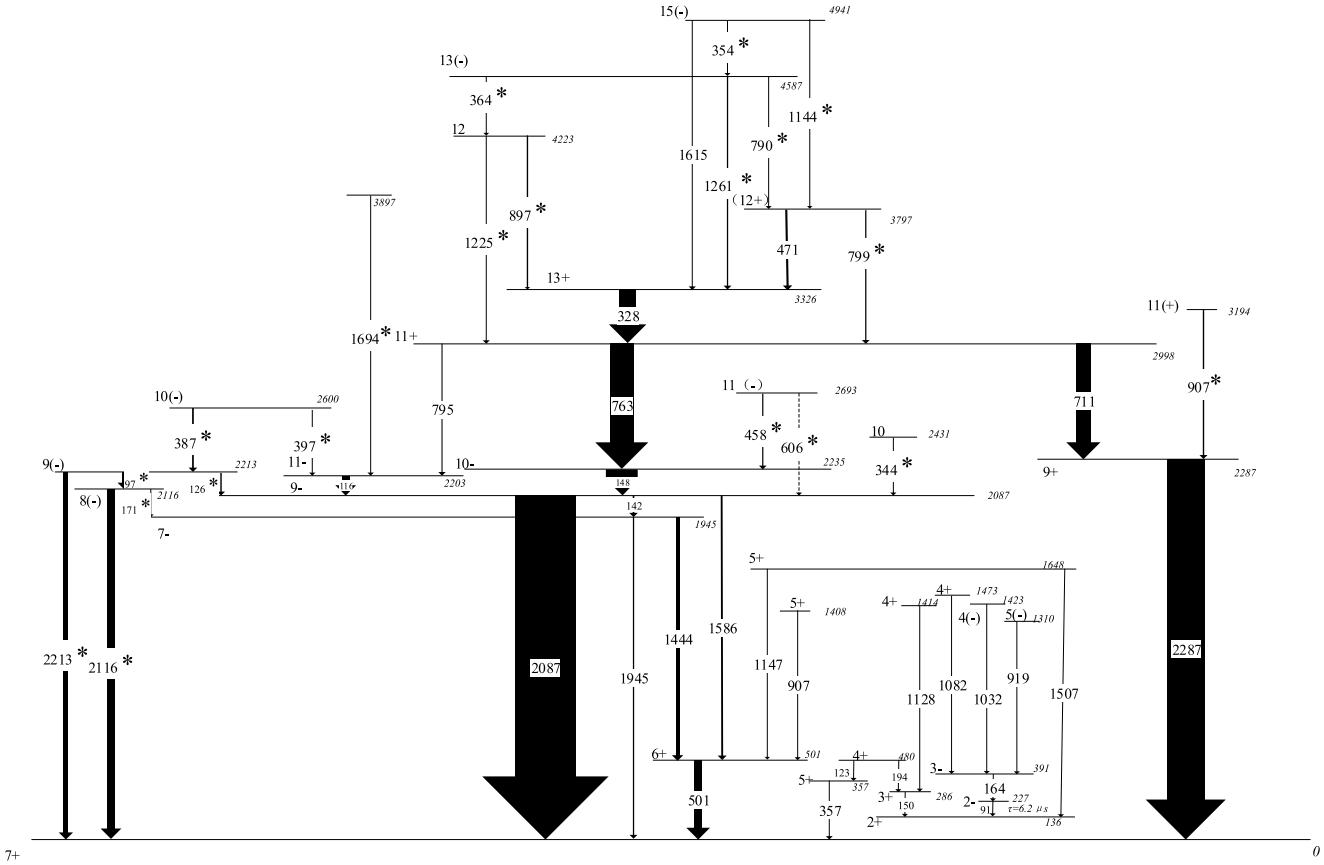

Fig. 2. Level scheme of ^{92}Nb proposed by the present work. New transitions are denoted with asterisks. The width of arrows indicates relative intensity of γ-rays.

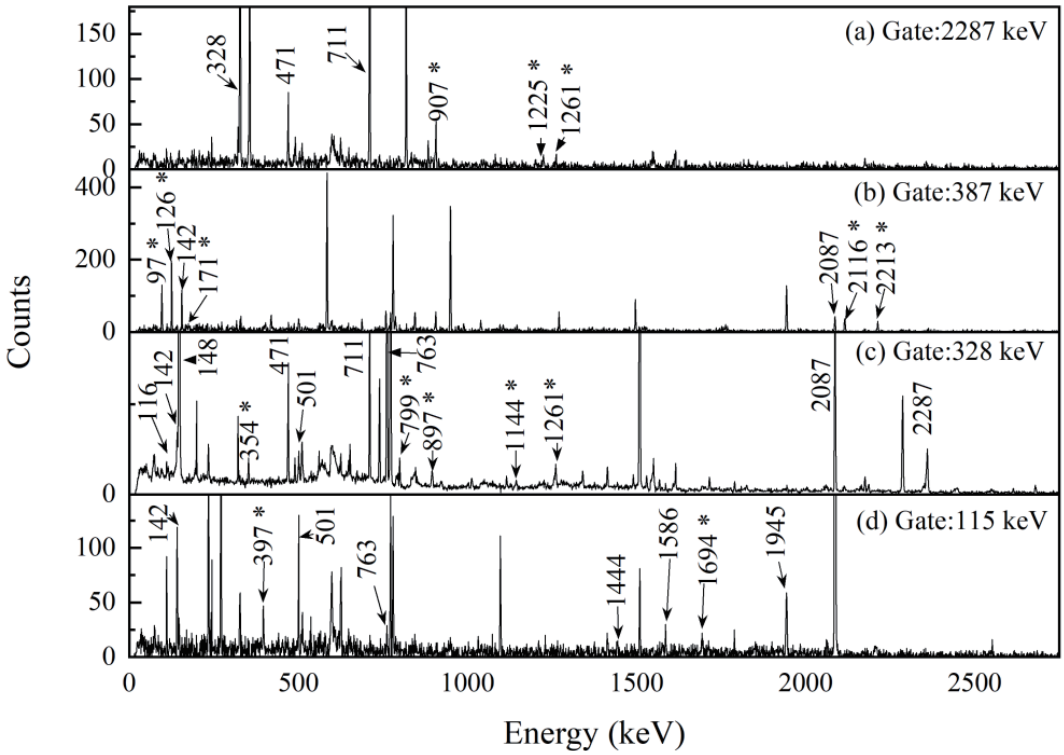

Fig. 3. Typical prompt γ-γ coincidence spectra for ^{92}Nb, gated on 2287, 387, 325, and 115 keV, respectively.

Table 1. Transition energies (E_γ) of ^{92}Nb, relative intensities of γ-rays (I_γ), initial and final states for γ-rays, ADO ratios, initial and final spins of the transitions.

E_γ /keV	I_γ [a]	$E_i^\pi \rightarrow E_f^\pi$	R_{ADO} [c]	$J_i^\pi \rightarrow J_f^\pi$
97*	8.79(159)	2213→2116	0.71(13)	$9^{(-)} \rightarrow 8^{(-)}$
116	15.08(80)	2203→2087	1.40(10)	$11^- \rightarrow 9^-$
126*	2.68(23)	2213→2087	1.58(25)	$9^{(-)} \rightarrow 9^-$
142	3.07(27)	2087→1945	1.63(33)	$9^- \rightarrow 7^-$
148	53.81(280)	2235→2087	0.94(5)	$10^- \rightarrow 9^-$
171*	0.49(18)	2116→1945	—	$8^{(-)} \rightarrow 7^-$
328	27.18(151)	3326→2998	1.52(9)	$13^+ \rightarrow 11^+$
344*	0.82(12)	2431→2087	0.96(23)	$10 \rightarrow 9^-$
354*	0.66(8)	4941→4587	1.46(37)	$15^{(-)} \rightarrow (13^-)$
364*	0.43(7)	4587→4223	0.96(30)	$(13^-) \rightarrow 12^{(-)}$
387*	3.03(41)	2600→2213	0.96(13)	$10^{(-)} \rightarrow 9^{(-)}$
397*	0.92(25)	2600→2203	0.94(36)	$10^{(-)} \rightarrow 11^-$
458*	1.92(18)	2693→2235	0.71(15)	$11^{(-)} \rightarrow 10^-$
471	3.53(25)	3797→3326	0.88(8)	$(12^+) \rightarrow 13^+$
501	12.77(180)	501→0	0.80(11)	$6^+ \rightarrow 7^+$
606*	W [b]	2693→2087	—	$11^{(-)} \rightarrow 9^{(-)}$
711	23.85(126)	2998→2287	1.80(11)	$11^+ \rightarrow 9^+$
763	39.35(168)	2998→2235	0.95(6)	$11^+ \rightarrow 10^-$
790*	0.66(11)	4587→3797	1.00(25)	$(13^-) \rightarrow (12^+)$
795	1.78(26)	2998→2235	—	$11^+ \rightarrow 11^-$
799*	2.07(26)	3797→2998	—	$(12^+) \rightarrow 13^+$
897*	1.67(76)	4223→3326	0.91(16)	$12^- \rightarrow 11^+$
907*	2.29(34)	3194→2287	1.78(49)	$11^{(+)} \rightarrow 9^+$
1144*	0.19(6)	4941→3797	—	$15^- \rightarrow (12^+)$
1225*	1.67(18)	4223→2998	0.95(46)	$12^{(-)} \rightarrow 11^+$
1261*	4.09(52)	4587→3326	1.51(20)	$(13^-) \rightarrow 13^+$
1444	5.05(62)	1945→501	0.94(12)	$7^- \rightarrow 6^+$
1586	3.09(45)	2087→501	—	$9^- \rightarrow 6^+$
1694*	W [b]	3897→2203	—	$\rightarrow 11^-$
1945	2.74(56)	1945→0	1.37(27)	$7^- \rightarrow 7^+$
2087	100	2087→0	1.40(8)	$9^- \rightarrow 7^+$
2116*	12.83(358)	2116→0	0.83(19)	$8^{(-)} \rightarrow 7^+$
2213*	7.67(170)	2213→0	1.66(67)	$9^{(-)} \rightarrow 7^+$
2287	61.98(367)	2287→0	1.66(14)	$9^+ \rightarrow 7^+$

[a] The errors of the relative intensity include the fitting and efficiency corrections. W[b] The intensities of transitions are too weak. [c] The errors of the ADO ratios include the fitting and efficiency corrections.

tensities of partial γ-rays from ^{93}Nb are given in Table 2.

4 Discussion

The excitation of a nearly spherical nucleus is usually considered to be of two types: single particle excitations inside a major shell, and excitations that cross the shell gap(s) [21]. The core excitation has been previously reported in A~90 neighboring nuclei, e.g., ^{89}Y [22], $^{91\text{-}94}$Mo [8, 23-25], and $^{94\text{-}96}$Ru [26], which exhibit the character-

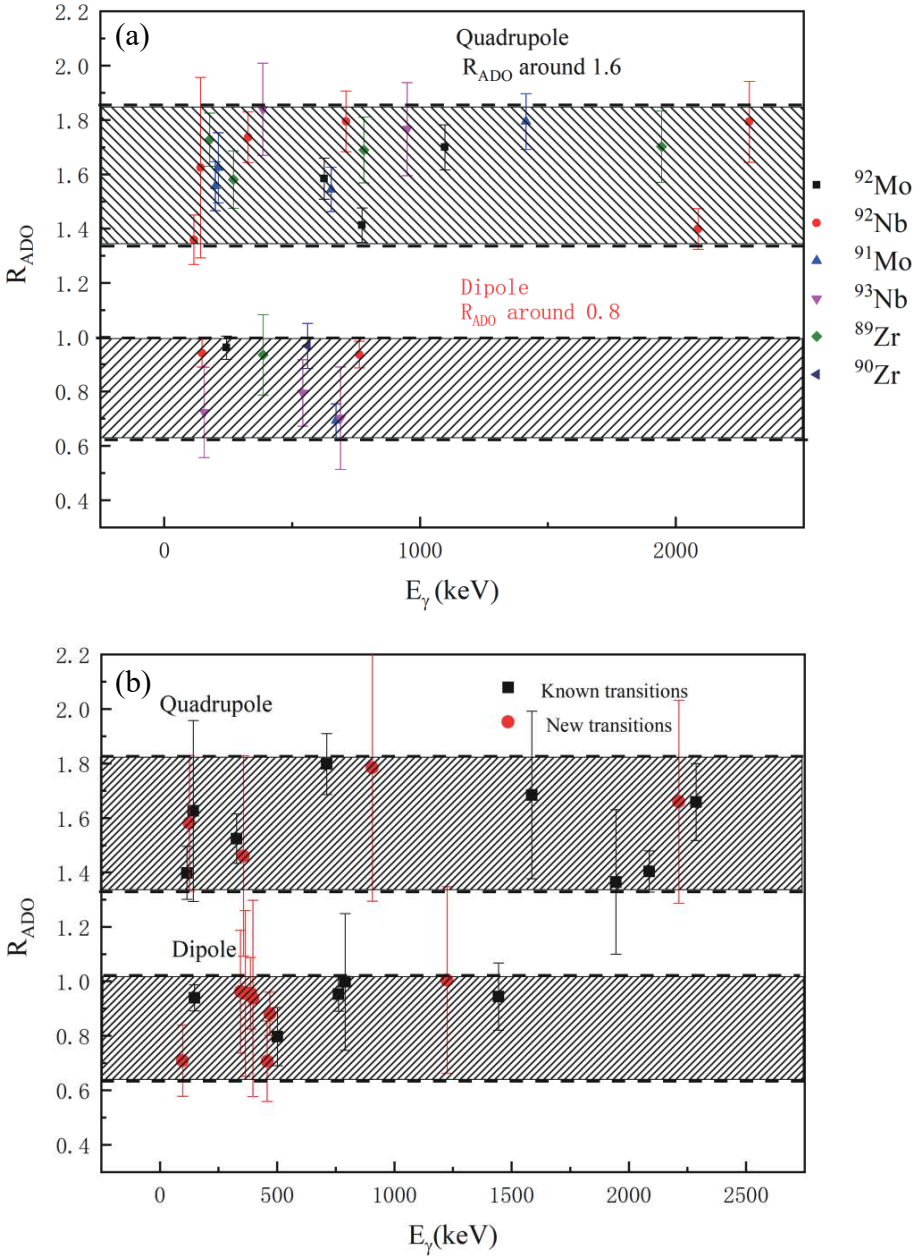

Fig. 4. (color online) (a) Representative ADO ratios in ^{92}Mo, ^{92}Nb, ^{91}Mo, ^{93}Nb, ^{89}Zr, ^{90}Zr. Typical R_{ADO} is given as around 1.6 indicating stretched quadrupole (or ΔI=0) transition, and around 0.8 indicating stretched dipole transition; (b) R_{ADO} of transitions plotted against energies of γ-rays in ^{92}Nb.

istics of several parallel transitions with energy around 2 MeV feeding into the same level. The low-lying states may be dominated by single particle excitations inside one major shell. As it is a nearly spherical nucleus, the states of ^{92}Nb should be amenable to shell model calculations.

In order to study the levels in ^{92}Nb, we performed shell model calculations with the code NushellX. The SNE model space and SNET interaction were adopted, which were previously used for level structures of nearly spherical nuclei ^{85}Br [27], ^{96}Ru [26], ^{94}Mo [8]. The model space includes 8 proton orbitals ($1f_{5/2}$, $2p_{3/2}$, $2p_{1/2}$, $1g_{9/2}$, $1g_{7/2}$, $2d_{5/2}$, $2d_{3/2}$, $3s_{1/2}$) and 9 neutron orbitals ($1f_{5/2}$, $2p_{3/2}$, $2p_{1/2}$, $1g_{9/2}$, $1g_{7/2}$, $2d_{5/2}$, $2d_{3/2}$, $3s_{1/2}$, $1h_{11/2}$) relative to the inert ^{56}Ni (Z = 28, N = 28) core.

The low-excited states of ^{92}Nb behave like single particle excitation, and thus we describe the low-excited states of ^{92}Nb as pure configurations, which means that each state corresponds to one proton orbital and one neutron orbital. The pure configuration calculations were also carried out for the low-excited states of ^{91}Zr, ^{93}Mo, ^{95}Ru [28]. Since the Fermi levels of ^{92}Nb lie at the $\pi g_{9/2}$ and

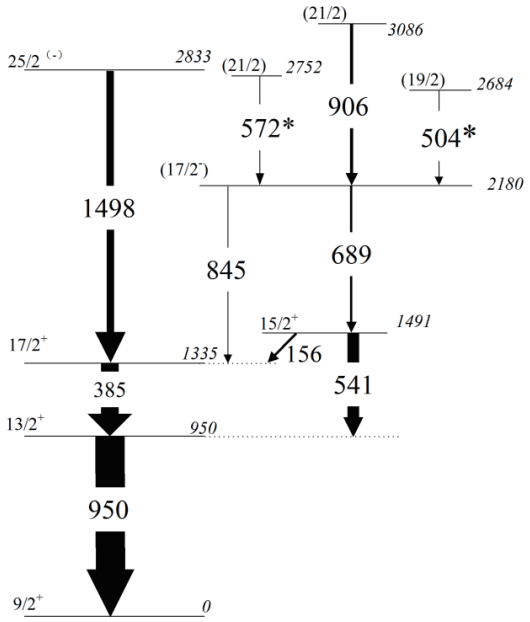

Fig. 5. Level scheme of ^{93}Nb proposed in the present work. New transitions are marked with asterisks. The width of the arrows indicates the relative intensity of γ-rays.

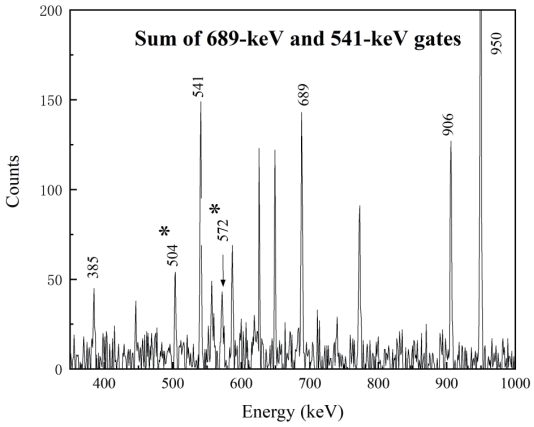

Fig. 6. Typical prompt γ-γ coincidence spectrum for ^{93}Nb with two new transitions marked with asterisks.

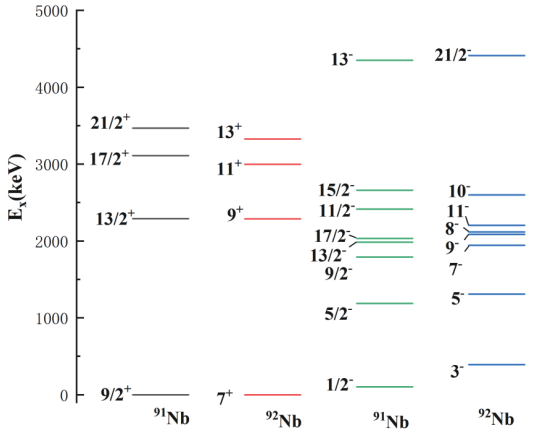

Fig. 7. (color online) Comparison of the low-lying states of ^{91}Nb and ^{92}Nb.

$\nu d_{5/2}$ orbitals, the quasi-magic nucleus ^{90}Zr is taken as the inert core to describe the low-lying states of ^{92}Nb, so that the $1f_{5/2}$, $2p_{3/2}$, $2p_{1/2}$ proton orbitals and the $1f_{5/2}$, $2p_{3/2}$, $2p_{1/2}$, $1g_{9/2}$ neutron orbitals are fully occupied. The first six positive parity states of ^{92}Nb ($I^{\pi}=2^{+}\sim7^{+}$) have been

Table 2. Transition energies (E_γ) of ^{93}Nb, relative intensities of γ-rays (I_γ), initial and final spins of the transitions.

E_γ/keV	I_γ[a]	$E_i^{\pi}\rightarrow E_f^{\pi}$	$J_i^{\pi}\rightarrow J_f^{\pi}$
156	8.1(19)	1491→1335	$15/2^{+}\rightarrow17/2^{+}$
385	58.8(69)	1335→950	$17/2^{+}\rightarrow13/2^{+}$
504*	2.8(6)	2684→2180	$(19/2)\rightarrow(17/2^{-})$
541	39.9(69)	1491→950	$15/2^{+}\rightarrow13/2^{+}$
572*	1.5(5)	2752→2180	$(21/2)\rightarrow(17/2^{-})$
689	7.1(21)	2180→1491	$(17/2^{-})\rightarrow15/2^{+}$
845	2.2(3)	2180→1335	$(17/2^{-})\rightarrow17/2^{+}$
906	10.8(24)	3086→2180	$(21/2)\rightarrow(17/2^{-})$
950	100	950→0	$13/2^{+}\rightarrow9/2^{+}$
1498	25.7(36)	2833→1335	$25/2^{(-)}\rightarrow17/2^{+}$

[a] The errors on the relative intensity include the fitting and efficiency corrections.

Table 3. Dominant configurations of the low-lying excited states of ^{92}Nb proposed by the shell model calculations with a pure configuration and SNET interaction, calculated results and experimental level energies.

I^{π}	configuration	E_{exp}/MeV	E_{cal}[1]/MeV
2^{+}	$\pi g_{9/2}\otimes\nu d_{5/2}$	0.136	0.326
3^{+}		0.286	0.402
4^{+}		0.480	0.495
5^{+}		0.357	0.372
6^{+}		0.501	0.515
7^{+}		0	0
2^{-}	$\pi(p_{1/2})^{-1}(g_{9/2})^{2}\otimes\nu d_{5/2}$	0.227	0.275
3^{-}		0.391	0.314
7^{-}		1.945	1.83
8^{-}		2.116	2.028
$9^{-}_{(1)}$		2.088	1.900
$9^{-}_{(2)}$		2.213	2.54
$10^{-}_{(1)}$		2.235	2.203
$10^{-}_{(2)}$		2.6	2.643
9^{+}	$\pi(p_{1/2})^{-2}(g_{9/2})^{3}\otimes\nu d_{5/2}$	2.287	2.552
11^{+}		2.998	3.295
12^{+}		3.797	3.859
13^{+}		3.326	3.528

[1] the result of shell model calculation with pure configurations.

previously interpreted as the $\pi(1g_{9/2})\otimes\nu(2d_{5/2})$ configuration, and the first two negative parity states of 2^- and 3^- are dominated by the $\pi(2p_{1/2})\otimes\nu(2d_{5/2})$ configuration [11, 13]. As ^{92}Nb has one neutron more than ^{91}Nb, it should have similar level structure for low-excited states, as shown in Fig. 7. Hence, the low-lying levels of ^{92}Nb are described as ^{91}Nb$\otimes\nu d_{5/2}$ as shown in Table 3, where the negative parity states $I^\pi=7^-$, 8^-, $9^-_{(1)}$, $9^-_{(2)}$, $10^-_{(1)}$, $10^-_{(2)}$ are described as a proton excited from the $p_{1/2}$ orbital to the $g_{9/2}$ orbital, and the positive parity states 9^+, 11^+, 12^+, 13^+ are described as a pair of protons excited from the $p_{1/2}$ orbital to the $g_{9/2}$ orbital. The calculation results for the one proton-neutron coupled configuration, $\pi g_{9/2}\otimes\nu d_{5/2}$, and for the two proton-hole neutron-particle coupled configuration, $\pi p_{1/2}^{-1}(g_{9/2})^2\otimes\nu d_{5/2}$ and $\pi(p_{1/2})^{-2}(g_{9/2})^3\otimes\nu d_{5/2}$, are listed in Table 3. As can be seen from this table, the shell model predictions for the low-excited states agree well with the experimental data, which confirms the assignments of Ref. [13] , where the first six positive parity states $I^\pi=2^+\sim7^+$ and the first two negative parity states 2^- and 3^- are $\pi g_{9/2}\otimes\nu d_{5/2}$ and $\pi p_{1/2}^{-1}(g_{9/2})^2\otimes\nu d_{5/2}$, respectively.

For the higher excited states of ^{92}Nb, ^{90}Zr is not an ideal core anymore, which makes the configuration of the high-excited states more complicated, as the pure configurations cannot describe the high-excited states properly. In order to study the high-excited states of ^{92}Nb, a large-basis shell model calculation is necessary.

To obtain a more appropriate description of the observed high-excited states of ^{92}Nb, large-basis shell model calculations are used. ^{92}Nb has 13 valence protons and 23 valence neutrons outside the ^{56}Ni core. Due to the large number of active orbitals, truncation of the model space is necessary. In the calculations of ^{92}Nb, the valance space is restricted to $\pi(1f_{5/2}^{4\text{-}6}, 2p_{3/2}^{2\text{-}4}, 2p_{1/2}^{0\text{-}2}, 1g_{9/2}^{1\text{-}6}, 1g_{7/2}^{0\text{-}0}, 2d_{5/2}^{0\text{-}0}, 2d_{3/2}^{0\text{-}0}, 3s_{1/2}^{0\text{-}0})\otimes(1f_{5/2}^{6\text{-}6}, 2p_{3/2}^{4\text{-}4}, 2p_{1/2}^{2\text{-}2}, 1g_{9/2}^{9\text{-}10}, 1g_{7/2}^{0\text{-}1}, 2d_{5/2}^{0\text{-}2}, 2d_{3/2}^{0\text{-}0}, 3s_{1/2}^{0\text{-}0}, 1h_{11/2}^{0\text{-}1})$. A comparison between the experimentally determined excitations and the large-basis shell model results is shown in Table 4.

Table 4. Main partition of the wave function for high-spin states of ^{92}Nb. Each angular momentum is composed of several different partitions. Each partition is of the form $p=\pi[p(1), p(2), p(3), p(4)]\otimes\nu[n(1), n(2), n(3), n(4), n(5), n(6), n(7), n(8), n(9), n(10)]$, where $p(i)$ represents the number of valence protons in the $1f_{5/2}$, $2p_{3/2}$, $2p_{1/2}$ and $1g_{9/2}$ orbitals, and $n(j)$ represents the number of valence neutrons in the $1f_{5/2}$, $2p_{3/2}$, $2p_{1/2}$, $1g_{9/2}$, $1g_{7/2}$, $2d_{5/2}$ $2d_{3/2}$ $3s_{1/2}$ $1h_{11/2}$ orbitals, respectively. One neutron is excited to the $g_{7/2}$ and $h_{11/2}$ orbitals in these calculations.

I^π	E_{exp} /MeV	E_{cal}[2]/MeV	configuration	partition(%)
9^+	2.287	2.111	6 4 0 3⊗6 4 2 10 0 1 0 0 0	50.24
			4 4 2 3⊗6 4 2 10 0 1 0 0 0	13.84
11^+	2.998	3.146	6 4 0 3⊗6 4 2 10 0 1 0 0 0	58.88
12^+	3.797	3.746	6 4 0 3⊗6 4 2 10 0 1 0 0 0	64.89
13^+	3.326	3.325	6 4 0 3⊗6 4 2 10 0 1 0 0 0	61.88
8^-	2.116	2.320	6 4 0 3⊗6 4 2 10 0 0 0 0 1	38.79
			6 4 2 1⊗6 4 2 10 0 0 0 0 1	21.59
9^-	2.088	2.232	6 4 0 3⊗6 4 2 10 0 0 0 0 1	30.85
			6 4 2 1⊗6 4 2 10 0 0 0 0 1	12.36
$9^-_{(2)}$	2.213	2.777	6 4 1 2⊗6 4 2 10 0 1 0 0 0	52.03
10^-	2.235	1.863	6 4 0 3⊗6 4 2 10 0 0 0 0 1	41.57
$10^-_{(2)}$	2.6	2.841	6 4 1 2⊗6 4 2 10 0 1 0 0 0	49.4
13^-	4.587	4.797	6 4 0 3⊗6 4 2 10 0 0 0 0 1	31.97
15^-	4.941	5.207	6 4 0 3⊗6 4 2 10 0 0 0 0 1	65.92

[2] the result of shell model calculation with mixed configurations.

5 Conclusions

Excited states of ^{92,93}Nb were studied in the reactions induced by the weakly-bound nucleus ^{6}Li. The states of ^{92}Nb were populated in the ^{89}Y(^{6}Li, $p2n$)^{92}Nb and ^{89}Y(α, n)^{92}Nb reactions, and of ^{93}Nb in the ^{89}Y(^{6}Li, pn)^{93}Nb reaction. A total of 20 new transitions, 8 new states of ^{92}Nb and two transitions in ^{93}Nb were observed and added to the level schemes of the two nuclei. The multipolarity of the states of ^{92,93}Nb was analyzed following the ADO ratio. Shell model calculations were performed with the code NushellX to reconstruct the level structure of ^{92}Nb,

where SNE valence space and SNET interaction were used. For the low-excited states, a pure configuration with ^{90}Zr as an inert core was employed. Large-basis shell model calculations were performed to study the higher excited states of ^{92}Nb. The results agree well with the experimental data.

We are grateful to the INFN-LNL staff for providing stable ^{6}Li beam throughout the experiment. This research was also supported by the HIRFL User Project, CAS.

References

1 S. Ali, T. Ahmad, K. Kumar et al, Eur. phys. J. A, **54**: 56 (2018)
2 B. B. Back, H. Esbensen, C. L. Jiang et al, Rev. Mod. Phys., **86**: 44 (2014)
3 L. F. Canto, P. R. S. Gomes, R. Donangelo et al, Phys. Rep.-Rev. Sec. Phys. Lett., **596**: 1-86 (2015)
4 L. F. Canto, P. R. S. Gomes, R. Donangelo et al, Phys. Rep.-Rev. Sec. Phys. Lett., **424**: 1-111 (2006)
5 M. Sinha, J. Lubian, Eur. phys. J. A, **53**: 224 (2017)
6 G.L. Zhang, G.X. Zhang, S.P. Hu et al, Phys. Rev. C, **97**: 014611 (2018)
7 S. P. Hu, G. L. Zhang, G. X. Zhang et al, Nucl. Instrum. Methods Phys. Res. Sect. A-Accel. Spectrom. Dect. Assoc. Equip., **914**: 64-68 (2019)
8 B. Kharraja, S. S. Ghugre, U. Garg et al, Phys. Rev. C, **57**: 2903-2911 (1998)
9 S. Shuifa, F. Keming, G. Jiahui et al, Eur. Phys. J. A, **32**: 149-158 (2007)
10 S. Cochavi, D.B. Fossan, Phys. Rev. C, **3**: 275-281 (1971)
11 I. Kumabe, S. Matsuki, S. Nakamura et al, Nucl. Phys. A, **218**: 201-212 (1974)
12 M. A. Rumore, C. A. Fields, J. J. Kraushaar, Nucl. Phys. A, **445**: 408-418 (1985)
13 J. B. Ball, M. R. Cates, Phys. Lett. B, **25**: 126-128 (1967)
14 B. A. Brown, D. B. Fossan, Physical Review C, **15**: 2044-2051 (1977)
15 Y. H. Wu, J. B. Lu, P. W. Luo et al, Chin. Phys. Lett., **31**: 3 (2014)
16 C. J. McKay, J. N. Orce, S. R. Lesher et al, Eur. Phys. J. A, **25**: 773-773 (2005)
17 Y. Wakabayashi, T. Fukuchi, Y. Gono et al, J. Phys. Soc. Jpn., **76**: 7 (2007)
18 J. J. V.-D.et al, INFN-LNL Annual Report, **241**: 95 (2015)
19 D. Testov, D. Mengoni, A. Goasduff et al, Eur. Phys. J. A, **55**: (2019)
20 M. F. Guo, G. L. Zhang, P. R. S. Gomes et al, Phys. Rev. C, **94**: 044605 (2016)
21 H. -K. Wang, S. K. Ghorui, K. Kaneko et al, Phys. Rev. C, **96**: 054313 (2017)
22 Z. Q. Li, S. Y. Wang, C. Y. Niu et al, Phys. Rev. C, **94**: 014315 (2016)
23 S. Ray, N. S. Pattabiraman, R. Goswami et al, Phys. Rev. C, **69**: 8 (2004)
24 N. S. Pattabiraman, S. N. Chintalapudi, S. S. Ghugre et al, Phys. Rev. C, **65**: 044324 (2002)
25 T. Fukuchi, Y. Gono, A. Odahara et al, Eur. Phys. J. A, **24**: 249-257 (2005)
26 S.S.G. B. Kharraja, *, R.V.F.J. and U. Garg, M. P. Carpenter, B. Crowell, † T. L. Khoo, T., a.D.N. Lauritsen, W. Reviol, W. F. Mueller, ‡ and L. L. Riedinger, R. et al, Phys. Rev. C, **57**: (1998)
27 R. J. Guo, Z. Q. Li, C. Liu et al, Chin. Phys. C, **41**: 4 (2017)
28 K. L. Wang, Y. H. Qiang, M. L. Liu et al, Nucl. Phys. Rev., **34**: 699-704 (2017)